P-13-11

The deep borehole concept

A conceptual model for gas generation and gas transport

Bertil Grundfelt, James Crawford
Kemakta Konsult AB

May 2014

Svensk Kärnbränslehantering AB
Swedish Nuclear Fuel
and Waste Management Co

Box 250, SE-101 24 Stockholm
Phone +46 8 459 84 00

ISSN 1651-4416
SKB P-13-11
ID 1401002

The deep borehole concept

A conceptual model for gas generation and gas transport

Bertil Grundfelt, James Crawford
Kemakta Konsult AB

May 2014

Summary

In the concept for deep borehole disposal of spent nuclear fuel developed by Sandia National Laboratories, the fuel is assumed to be encapsulated in mild steel canisters and stacked at 3–5 km depth in boreholes. In this disposal zone, the boreholes are cased with perforated mild steel casing tubes. In this study, a conceptual model has been developed for the generation of hydrogen gas by corrosion of the canisters and casing tubes. The model is first derived for a borehole that is compartmentalised by concrete plugs at regular intervals in the borehole. This model is then simplified to comply with the described case with a perforated casing that leads to a short-cutting of the compartmentalisation. The model is based on anaerobic corrosion reaction between iron and water in which magnetite (Fe_3O_4) and hydrogen gas are formed. It is demonstrated that the equilibrium hydrogen pressure, i.e. the hydrogen pressure at which the corrosion reaction stops, is likely to significantly exceed the hydrostatic pressure at the depth where the canisters are assumed to be disposed. The consequence of this is that gas bubbles will form at the corroding iron surfaces.

The gas bubbles formed will displace an equal volume of borehole fluid into fractures in the adjacent rock. If the gas pressure exceeds the sum of the hydrostatic pressure and the capillary pressure in the rock matrix the gas may also start to displace water in the rock matrix. When detached from the corroding surface the bubbles will strive upwards and create a head space below the nearest concrete plug. The corrosion rate in this head space will proceed relatively unhindered since there will always be a liquid water film at the corroding metal surface due to water vapour diffusive transport. In practice, it is likely that there will be a partially water saturated boundary zone between the head space and the fully water saturated zone at the bottom of the borehole compartment.

A mathematical model is derived for the equilibrium hydrogen partial pressure as a function of borehole depth and temperature. The model assumes that the displaced borehole fluid flows efficiently into fractures in the adjacent rock or upwards through the borehole so that gas is generated in the borehole at a rate determined by the difference in the local hydrostatic pressure and equilibrium partial pressure at that temperature.

Using a range of corrosion rates for mild steel reported in the literature, the estimated overall rate of hydrogen formation corresponds to 0.19–186 m^3 NTP (normal temperature and pressure) per year from the disposal zone (3–5 km depth) of one borehole depending on the type of steel used in construction. In the warm and saline borehole environment a value in the upper part of the interval would be expected. Neglecting the reaction rate limitation obtained from the hydrogen pressure developing yields an approximately 70% higher gas formation rate. The calculations suggest that the entire water content in the borehole annulus can be displaced by free phase hydrogen in slightly more than 100 years assuming a corrosion rate in the upper part of the interval given above and including the time required to establish a steady-state concentration of dissolved hydrogen.

The amount of gas in the borehole will increase along the length of the borehole when bubbles formed higher up add to the rising bubbles. Also, because of the strong variation of the hydrostatic pressure over the length of the borehole, bubbles will expand as they rise. It is likely that a significant amount of the gas formed will be dissipated through the rock adjacent to the borehole. As the rock around the borehole is likely to be affected by rock fallout and deformation due to anisotropic rock stresses, there will be a space between the casing and the rock wall that is available for upward flow of gas. The consequences in terms of displacement of groundwater and borehole liquid, possibly contaminated with radionuclides, remain to be analysed. The flow situation is complicated to treat computationally. Normally the necessary simplifications include assuming that the bubbles are non-deformable, non coalescing spheres and that the hydrodynamic problem is treated as a single phase flow.

Sammanfattning

Det koncept för slutförvaring av använt kärnbränsle som tagits fram av Sandia National Laboratories innebär att bränsleelementen kapslas in i kolstålskapslar som staplas på varandra på mellan 3 och 5 kilometers djup i borrhål. I deponeringszonen är borrhålet försett med perforerade foderrör. I denna studie har en konceptuell modell för vätgasbildning från korrosion av kapslar och foderrör utvecklats. Modellen utvecklas först för ett borrhål som delas upp av betongproppar i lika långa intervall. Denna modell förenklas sedan för att överensstämma med den beskrivna anläggningsutformningen med perforerade foderrör varigenom intervallindelningen av borrhålet kortsluts. Modellen grundas på anaerob korrosion i vilken järn och vatten reagerar under bildning av vätgas och magnetit (Fe_3O_4). Det visas att vätgasens jämviktstryck i denna reaktion, dvs det vätgastryck vid vilket korrosionsreaktionen avstannar, sannolikt väsentligt överskrider det hydrostatiska trycket på deponeringsdjupet. Konsekvensen blir att gasbubblor bildas på de korroderande järnytorna.

Gasbubblorna som bildas förtränger en lika stor volym borrhålsvätska till sprickorna i det omgivande berget. Om gastrycket överskrider summan av kapillärtrycket i bergmatrisen och det hydrostatiska trycket kan gasen även börja förtränga vattnet i bergmatrisen. När gasbubblorna frigörs från den korroderande järnytan kommer de att sträva uppåt och samlas under den närmaste betongproppen varvid en fri gasvolym bildas. Korrosionen fortgår dock även i denna gasvolym eftersom det nära stålytorna alltid kommer att finnas åtminstone en film av vatten som kan reagera med järnet. I praktiken kommer det att utbildas en partiellt vattenmättad övergångszon mellan den fria gasvolymen och den kontinuerliga vattenfasen.

En matematisk modell har utvecklats som beskriver utvecklingen av vätgastrycket som funktion av borrhålets djup och temperatur. Modellen baseras på antagandet att den förträngda borrhålsvätskan strömmar effektivt ut i berget eller uppåt i borrhålet så att gas bildas i borrhålet med den hastighet som bestäms av skillnaden mellan det lokala hydrostatiska trycket och jämviktstrycket för korrosionsreaktionen.

Om man utgår från litteraturdata för kolstålskorrosionens kinetik och antar att trycket av den bildade vätgasen är lika med det hydrostatiska trycket vid bildningsdjupet får man en beräknad total vätgasbildning i deponeringszonen (3–5 km djup) motsvarande 0,19–186 Nm^3/år (normalkubikmeter vid atmosfärstryck och rumstemperatur). Ett värde i den övre delen av intervallet bedöms troligt vid de temperaturer och salthalter som förväntas i deponeringszonen. Om den begränsning av reaktionshastigheten som fås från den bildade vätgasen försummas fås en cirka 70 % högre gasbildningstakt. Beräkningarna visar att den tid som behövs för att med den bildade vätgasen förtränga vattnet i spalten mellan kapslarna och borrhålsväggen uppgår till drygt 100 år inklusive den tid det tar att först mätta vattnet på löst vätgas.

Gasmängden i borrhålet kommer att öka uppåt när bubblor som bildas högre upp läggs till de stigande gasbubblorna. Den stora variationen av hydrostatiskt tryck längs med borrhålet medför också att gasbubblorna expanderar när de stiger. Det är troligt att en väsentlig del av den bildade gasen kommer att spridas genom sprickorna i det omkringliggande berget. Då berget närmast borrhålet sannolikt är påverkat av bergutfall och deformerat på grund av anisotropa bergspänningar kommer det att finnas ett utrymme mellan foderröret och hålets bergrum där gasen kan röra sig uppåt. Det återstår att utreda konsekvenserna i form av förträngning av potentiellt radionuklidkontaminerat grundvatten. Den hydrodynamiska situationen är beräkningsmässigt komplicerad att behandla. Nödvändiga förenklingar omfattar normalt antaganden om att bubblorna är stela sfärer som inte kan slås ihop och att det hydrodynamiska problemet kan behandlas som enfasflöde.

Contents

1 Introduction

Disposal of nuclear waste in deep (~5 km) boreholes has been discussed since at least the 1970s. At the end of the 1980s and the beginning of the 1990s SKB developed and evaluated a conceptual design for deep borehole disposal based on 0.5 m wide cylindrical canisters hosting up to four spent BWR fuel elements or one PWR-element (SKB 1992). The weakness of this concept was the 80 cm wide boreholes needed to dispose of such big canisters that, at least at the time of the study, were beyond the capabilities of the drilling industry. Recently the Sandia National Laboratories, SNL, developed a reference design based on 43 cm boreholes (Arnold et al. 2011). As this aligns with a developing consensus that up to 0.5 m wide boreholes, although such holes have not yet been drilled, should be possible to construct based on existing technology (Beswick 2008).

SKB has decided to base any further work on deep borehole disposal on a modification of the SNL reference design using slightly wider 44.5 cm boreholes. The boreholes are assumed to be lined with a mild steel casing. The casing is expected to sit not entirely flush with the borehole and there is space on the inner and outer side of the liner that would be filled with drilling mud to prevent borehole breakouts caused by the great stresses encountered at depths of down to 5 km. The spent fuel is assumed to be encapsulated in mild steel canisters that are joined together by couplings to form 200 m long strings of that are stacked in the section of the borehole between 3 and 5 km depth.

The main safety function of a deep borehole repository is the anticipated very slow groundwater movements at depth caused by a density stratification caused by the salinity of deep groundwater in combination with low rock permeability. Since both the borehole casing and the canisters are assumed to be made of mild steel, the question has been raised if corrosion of the metal surfaces will create significant amounts of hydrogen that could disrupt the stability of the density stratification and hence the stagnancy of the deep groundwater.

In the case with a perforated casing, there will a free upward flow of gas bubbles through the annulus between the casing and borehole wall. It is conceptualised that discrete bubbles of H_2 gas will form at the steel surfaces as corrosion proceeds. When the buoyancy force acting on an individual bubble exceeds the surface adhesive force for the bubble to remain in contact with the surface, it may detach and flow upwards through the borehole mud.

In this process, one can envisage that bubbles will detach continuously along the length of the corroding metal in the borehole, adding to the existing population of bubbles rising through the fluid. Bubbles may also coalesce depending on the size of the individual bubbles and interphase surface forces. Above a certain cross-sectional gas flow (loading), bubble coalescence may lead to slug flow and eventually free phase flow if the gas production rate is sufficiently high. The hydrodynamic drag associated with the rising plume of bubbles will cause pressure gradients along the borehole, which may lead to water being drawn into the borehole from the surrounding permeable rock. On the other hand, if the transport capacity in the borehole is too low for the gas generated, gas may enter into the fractures in the adjacent rock thereby creating driving forces for upward groundwater movement. If the gas production is sufficiently rapid over the timescale being considered and the borehole sealing devices fail, there is also the risk of an extrusion of borehole contents at the surface.

This report describes a conceptual model for the gas evolution and gas transport in deep borehole disposal of spent nuclear fuel based on anoxic corrosion of the casing and the canisters involving reduction of water with consequent formation of H_2 gas. The model is used to perform scoping calculations of the equilibrium hydrogen pressure and of the amount of hydrogen formed by the corrosion processes.

In Chapter 2 a description of the borehole design and the disposal procedure assumed is given. Following this, a description of the chemistry of the corrosion and gas production reactions is given in Chapter 3 and an assessment is made of the equilibrium hydrogen pressure in Chapter 4. In Chapter 5, a simplified mathematical model of the rate of hydrogen formation is developed and applied to an approximate calculation of the volume of hydrogen gas formed in a borehole. In Chapter 6, possibilities to model the dynamics of the gas transport through the borehole fluid are discussed.

2 Borehole design and disposal procedure

The present study is based on a borehole design and procedures for construction, operation and closure originally proposed by Arnold et al. (2011) but with a 44.5 cm (17½”) borehole diameter (Odén 2013). The extra 0.5-inch borehole diameter allows the use of a slightly larger canister that could host one PWR or two BWR fuel elements without fuel element consolidation. The boreholes should be drilled using directional drilling such that they are straight and vertical with only minor deviations from the vertical directions (<0.5°). The facility design and key dimensions are shown in Figure 2-1 and Table 2-1. The table also shows the number of canisters needed for disposal of the spent fuel from the current Swedish nuclear programme.

The spent fuel is placed in steel canisters. During disposal strings of 40 canisters are joined together by couplings and lowered to the disposal zone located between three and five kilometres depth using the drilling rig with its drill stem. When a canister string has been emplaced in the hole, a bridge plug is placed above the string and a 10 metres long concrete plug is cast on top of the bridge plug. The concrete plug will then function as the floor of the next canister string. In this way, ten canister strings can be disposed of in the two kilometres long disposal zone. A facility designed for disposal of all spent fuel from the current Swedish nuclear programme would consist of about 80 deposition holes.

During disposal the borehole is filled with a borehole mud. The casing is perforated in the disposal zone, in order to avoid differential hydrostatic pressure and to ensure that the borehole mud fills the annulus between the casing and the wall of the borehole. Before each disposal operation, the hole will be monitored with a caliper tool, in order to detect any deformation that might infringe on the possibility for a successful disposal. Also, each canister string will be equipped with a calliper tool at the bottom end so that constrictions in the borehole can be detected.

When all 10 canister strings have been emplaced, a bridge plug is inserted over the last canister string and a 100 metres long concrete plug is cast on top of the bridge plug. The borehole is then sealed following a procedure described by Odén (2013). The procedure includes the removal of the portion of the 406 mm casing above the concrete plug and the part of the 473 mm casing above cementation followed by filling the hole with alternating concrete, bentonite, gravel and possibly asphalt plugs (Odén 2013).

Table 2-1. Key dimensions of a deep borehole disposal facility.

Design parameter	Value
Borehole diameter in the disposal zone	445 mm
Casing dimensions in the disposal zone	OD = 406 mm, ID = 381 mm
Canister outer diameter	340 mm
Canister inner diameter	318 mm
Outer diameter of canister couplings	360 mm
Canister capacity, number of fuel elements	1 PWR or 2 BWR
Number of canisters, BWR fuel + PWR fuel=total	25,350+7,090=32,440

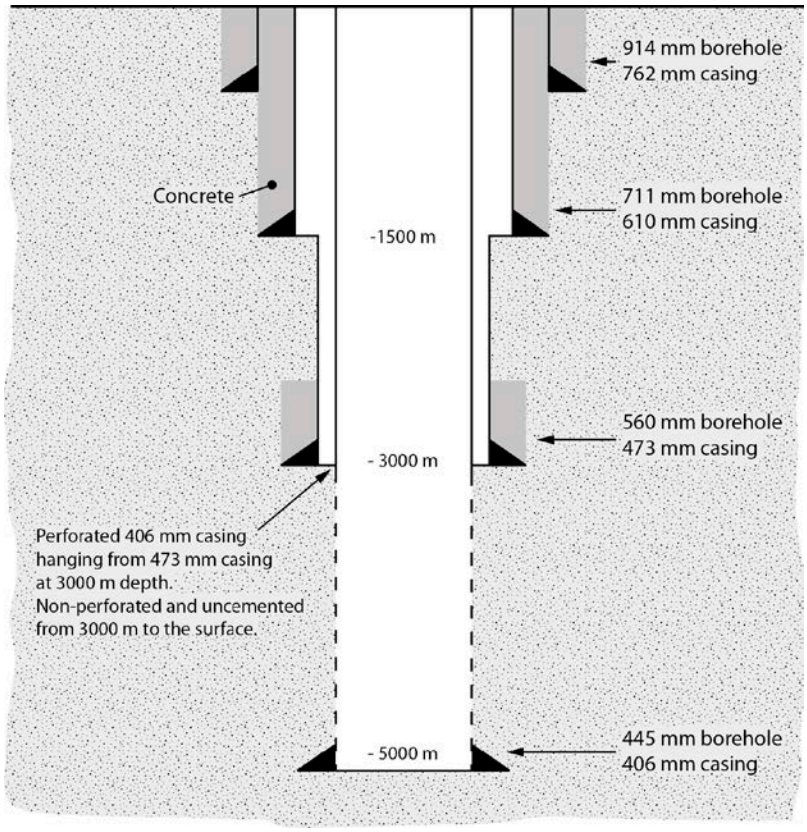

Figure 2-1. *Conceptual design of a facility for disposal of spent nuclear fuel in deep boreholes(not to scale), after Odén (2013).*

3 Gas production chemistry

The most likely corrosion reactions involving carbon steel (C-steel) under anoxic conditions are (Reardon 1995, Ortiz et al. 2002):

$$Fe_{(cr)} + 2H_2O \leftrightarrow Fe^{2+} + 2OH^- + H_{2(g)} \quad (3\text{-}1)$$

$$Fe_{(cr)} + 2H_2O \leftrightarrow Fe(OH)_2 + H_{2(g)} \quad (3\text{-}2)$$

$$Fe_{(cr)} + \tfrac{4}{3}H_2O \leftrightarrow \tfrac{1}{3}Fe_3O_{4(s)} + \tfrac{4}{3}H_{2(g)} \quad (3\text{-}3)$$

In groundwater with significant amounts of dissolved carbonate, the following reaction might also need to be considered:

$$Fe_{(cr)} + H_2CO_3 \leftrightarrow FeCO_3 + H_{2(g)} \quad (3\text{-}4)$$

The ferrous hydroxide product (3-2) is only metastable and generally the magnetite reaction product (3-3) is expected in deep groundwater systems. As the reaction progresses the equivalent partial pressure of H_2 increases until it exceeds the local hydrostatic pressure at which point gas bubbles form spontaneously. Based on Le Chatelier's principle, the increase in H_2 partial pressure will shift the reaction to the left and corrosion will cease once the equilibrium partial pressure is attained. The equilibrium partial pressure, however, will be some tens of MPa depending on the groundwater chemical composition and temperature. For much of the borehole interval at canister emplacement depth, the equilibrium partial pressure may therefore be higher than the local hydrostatic pressure thus permitting relatively unhindered gas generation.

In the deep borehole disposal concept, concrete plugs at regular intervals are intended to carry the load of the canisters above and will also isolate discrete sections within the steel casing. The volume of gas that is generated will displace an equal volume of water which may be displaced through connected fractures that happen to intersect the borehole. The slot between the outer casing and the borehole wall will not be plugged and therefore will provide a vertical flowpath for transport of gas bubbles. Gas may also enter fractures in the adjacent rock giving rise to driving forces for upward groundwater flow. If the gas cannot escape and the pressure build-up in the borehole exceeds the sum of hydrostatic pressure and capillary pressure in the rock matrix, gas may also be forced advectively through the rock matrix.

4 Estimation of the equilibrium H_2 partial pressure

4.1 Electrochemical considerations

The upper limit to the theoretical H_2 partial pressure that can be reached is set by the mass action relations for the corrosion reactions. Corrosion is the net result of the balanced combination of oxidation and reduction half-cell reactions. The relevant electrochemical reactions for various possible corrosion processes involving C-steel are given in Table 4-1.

For a generalised reduction reaction, the theoretical cell potential relative to the standard hydrogen electrode is given by the Nernst equation (e.g. Langmuir 1997):

$$E_{cell}\left(V_{SHE}\right) = E^0\left(V_{SHE}\right) + 2.303\frac{RT}{nF}\log_{10}\prod_{i=1}^{m} a_i^{v_i} \qquad (4\text{-}1)$$

Where a_i represents component activities, and v_i are the stoichiometric coefficients of the components of the reduction reaction. The activity of gaseous components is defined in terms of the fugacity, f. The fugacity is the equivalent pressure of an ideal gas, which would give the same chemical potential as the real gas in the equilibrium reaction. The term E^0 is the standard potential of the half-reaction in volts (i.e. V_{SHE}, relative to the standard hydrogen electrode at 25°C and 1 atm.).

For corrosion to occur, the equilibrium potential for the anodic process (reactions 1–5) must be lower than the equilibrium potential for the cathodic process (reactions 6–8). The point of equivalence of an anodic and cathodic process corresponds to the equilibrium partial pressure of H_2 gas for that process. Assuming a groundwater with a constant pH 7, dissolved carbonate content of 42 mg/l, and dissolved Fe^{2+} activity of 10^{-6} M, the potentials for the anodic and cathodic processes can be computed simply using Equation 4-1 giving the characteristic curves shown in Figure 4-1 (activities of solution species are plotted in Figure 4-2).

Table 4-1. Electrochemical half-reactions for possible corrosion processes in deep reducing groundwater. Equilibrium constants, reaction enthalpies, and standard potentials are calculated based on data given in the SKB thermodynamic database, SKB-TDB (SKBdoc 1261302 ver 3.0), and Lemire et al. (2013).**

#	Reaction*	$\log_{10}K$	ΔH_r^0 (kJ/mol)	E_0 (V_{SHE})
1	$Fe^{2+} + 2e^- \rightarrow Fe_{(cr)}$	–15.86	90.0	–0.469
2	$FeCO_3 + 2e^- \rightarrow Fe_{(cr)} + CO_3^{2-}$	–26.75	79.62	–0.791
3	$FeCO_3 + H^+ + 2e^- \rightarrow Fe_{(cr)} + HCO_3^-$	–16.42	64.72	–0.486
4	$Fe(OH)_2 + 2H^+ + 2e^- \rightarrow Fe_{(cr)} + 2H_2O$	–11.52	–27.60	–0.082
5	$Fe_3O_4 + 8H^+ + 8e^- \rightarrow 3Fe_{(cr)} + 4H_2O$	–18.11	–23.93	–0.134
6	$H_2O + e^- \rightarrow ½H_{2\,(g)} + OH^-$	–13.9995	55.9045	–0.828
7	$H_2CO_3 + e^- \rightarrow ½H_{2\,(g)} + HCO_3^-$	–7.905	6.84	–0.468
8	$HCO_3^- + H^+ + e^- \rightarrow ½H_{2\,(g)} + CO_3^{2-}$	–10.33	14.90	–0.611

* All reactions written as reduction processes.

** SKB's internal database.

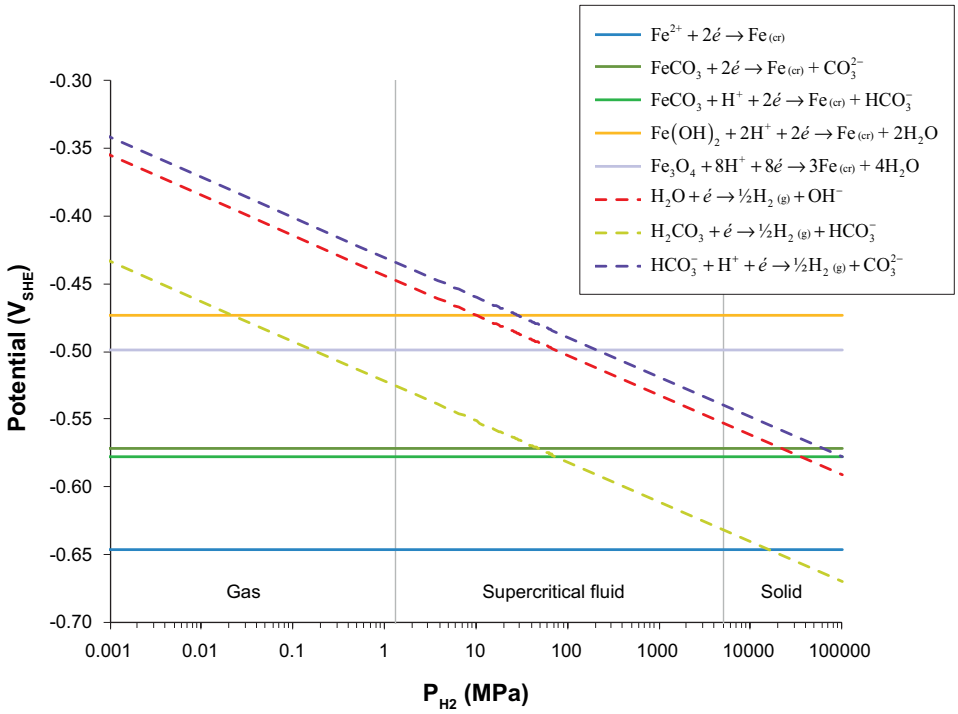

Figure 4-1. *Effect of H_2 partial pressure on equilibrium potential for anodic (unbroken lines) and cathodic (broken lines) processes given in Table 4-1 (assuming ideal gas). Calculations assume a temperature of 25°C, pH 7.0, an Fe^{2+} activity of 10^{-6}, and 42 mg/l dissolved carbonate. Approximate H_2 phase boundaries are also shown as vertical grey lines.*

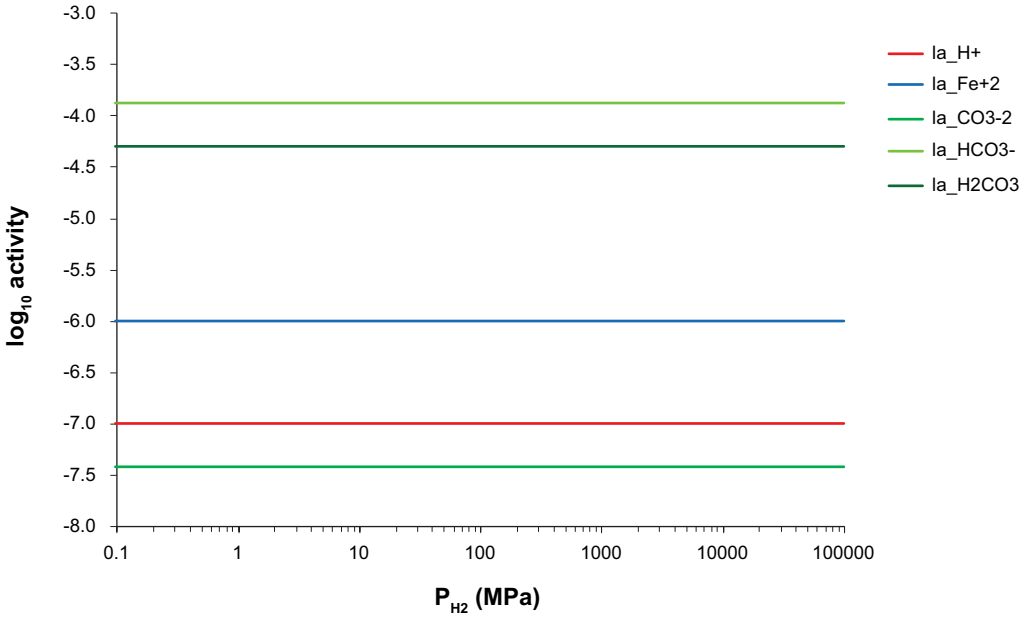

Figure 4-2. *Aqueous phase activities of groundwater components assumed in calculation of the Nernst potentials in Figure 4-1.*

The anodic processes (reactions 1–5) in Figure 4-1 are independent of H_2 gas partial pressure and therefore appear as horizontal lines. The cathodic processes (reactions 6–8), on the other hand, have a slope of –29.5 mV per decade increase in H_2 partial pressure. As can be seen from the curves, the formation of the metastable ferrous hydroxide phase, $Fe(OH)_2$ is unfavourable at pressures higher than about 10 MPa. Magnetite, Fe_3O_4 can form up to about 77 MPa assuming reduction of water (reaction 6) as the cathodic process. For the given pH and total carbonate concentration, corrosion processes involving siderite, $FeCO_3$, precipitation are possible at higher partial pressures, although these will be limited by the amount of dissolved carbonate. A free gas phase volume can only form if the partial pressure of H_2 gas exceeds the local hydrostatic pressure in the groundwater. According to this simplified analysis, the corrosion process resulting in Fe^{2+} (no mineral precipitate) is for all practical purposes unbounded suggesting that Fe corrosion resulting in the production of an H_2 gas phase will occur by reduction of water regardless of the prevailing hydrostatic pressure.

4.2 Calculation of the non-ideal equilibrium P_{H2} in a closed system

Although the simple calculations in the previous section show that corrosion is thermodynamically feasible at the in situ hydrostatic pressures expected at 5 km depth, the analysis does not consider non-ideality of the gas phase, elevated temperatures at great depth, nor changes in groundwater composition due to the corrosion occurring in a relatively closed system. In order to investigate the impact of these factors on the equilibrium partial pressure it is necessary to make numerical calculations using a suitable geochemical simulation code as is done in this section.

Since the hydrostatic pressure at storage depth will be on the order of 30 MPa or greater, H_2 cannot be assumed to behave as an ideal gas and an appropriate equation of state (EOS) must be chosen in order to calculate the fugacity. There are a number of different EOS models that can be used of which the Soave-Redlich-Kwong (SRK) and Peng-Robinson (PR) are the most commonly used in the engineering literature (e.g. Smith and Van Ness 1987). Version 3 of the PhreeqC geochemical simulation code (Parkhurst and Appelo 2013) has the capability of modelling gas phases using the PR-EOS if appropriate parameters are provided in the database, or otherwise defined in an input file.

At low temperatures and pressures, the activities of pure phases are set to unity by convention. At the elevated pressures encountered at depth in a deep borehole, however, the activities of both aqueous components and pure phases need to be calculated taking the influence of pressure into account. From the basic definition of Gibbs free energy, the change in the equilibrium constant for a reaction as a function of pressure at constant temperature is given by (Langmuir 1997):

$$\left(\frac{\partial \ln K}{\partial P}\right)_T = \frac{\Delta V_R^0}{RT} \tag{4-2}$$

Where, ΔV_R^0 is the net change in molar volume of reactants and products in the reaction at standard temperature and pressure. If the molar volume of reactants and products do not change in the pressure interval of interest, Equation 4-2 can be integrated to give a conditional equilibrium constant for the reaction as a simple function of pressure. In PhreeqC the conditional equilibrium constant is calculated (Appelo et al. 2014) using the relation:

$$\log_{10} K_{P,T} = \log_{10} K_{P_0,T} - \frac{\Delta V_R^0 \left(P - P_0\right)}{2.303RT} \tag{4-3}$$

At low to medium ionic strength the Truesdell-Jones (TJ) or Davies equations (both employed by PhreeqC) can be used to calculate aqueous phase activities (e.g. Langmuir 1997). These models give comparable results up to ionic strengths of about 0.7 mol/kg_w (roughly that of seawater), although they diverge significantly at higher ionic strengths. The Truesdell-Jones model is reasonably accurate up to about 2 mol/kg_w. At higher ionic strengths, activities need to be calculated either using the specific ion-interaction theory (SIT) or Pitzer models (e.g. Langmuir 1997).

All thermodynamic modelling calculations described in this report apart from the simplified Nernst analysis use the LLNL thermodynamic database (LLNL-TDB) distributed with the PhreeqC program (Parkhurst and Appelo 2012). This is a translation of the EQ3/6 database "thermo.com.V8.R6.230" produced at the Lawrence Livermore National Laboratory for use in geochemical calculations at elevated temperatures and pressures. This database is considered more internally consistent for reaction modelling at elevated temperatures than the SKB-TDB data used in the Nernst analysis. The equilibrium constants in Table 4-1 are not directly comparable with those given in the LLNL-TDB, however, since the LLNL-TDB entries are written in terms of dissolved O_2 gas as an oxidant instead of H_2 gas as in Table 4-1 and therefore require recalculation. The thermodynamic data from the SKB-TDB was preferred for the Nernst analysis at 25°C since redox half-reactions were defined more conveniently using the operational electron exchange formalism. The default activity model in PhreeqC is the Davies model unless Truesdell-Jones parameters are specified. The LLNL-TDB specifies ion specific interaction terms using the Truesdell-Jones activity model, although formulated slightly differently to other databases typically used with PhreeqC.

The groundwater composition assumed in the present calculations (see Table 4-2) is the same as the Brine (Type IV) groundwater described in Crawford (2008), although with sulphur species excluded to simplify interpretation. This composition is based on a deep groundwater sample taken from borehole KLX02 in the Laxemar site investigation area and is thought to be representative of a deep brine groundwater. The ionic strength of this groundwater is 1.52 mol/kg_w implying that activity corrections should be reasonably accurate provided significant increases in the dissolved concentration of solution components do not occur.

The corrosion process has been simulated with PhreeqC by adding incremental amounts of metallic $Fe_{(cr)}$ as a reaction and calculating the resulting equilibrium where ferrous hydroxide, siderite, and magnetite are permitted to precipitate if oversaturated. The partial pressure of H_2 gas is calculated assuming a constant volume process where the total pressure is initially 0.1 MPa (i.e. atmospheric pressure). The corrosion of $Fe_{(cr)}$ continues until the saturation index for both the metallic Fe reduction reaction and the precipitation of the corrosion product are simultaneously zero (i.e. where metallic $Fe_{(cr)}$ and the corrosion product can coexist at equilibrium). Since there is not an exact 1:1 relation between the number of moles of Fe reacted and those precipitated, there is a net increase in the amount of dissolved Fe^{2+} as the system approaches equilibrium which gives a significant increase in pH since water hydrolyses producing hydroxyl anions to balance the excess positive charge.

The presence of significant amounts of concrete in the compartmentalising plugs might further add to the pH increase due to their alkaline porewater content. The actual borehole cannot be considered a completely closed system, however, and some degree of pH buffering would most likely occur by diffusive exchange with unaffected water in the rock matrix, flow-bearing fractures intersecting the borehole section, as well as dissolution-precipitation reactions involving matrix minerals and borehole mud that fills the annular space in the deposition hole. Consideration of these additional processes would be more complex to model and therefore they have been neglected in the present scoping calculations.

Table 4-2. Deep brine groundwater composition used in calculations for C-steel corrosion. In order to simplify calculations the sulphate content of the groundwater has been neglected in this work. The ionic strength of this groundwater is initially 1.52 mol/kg_w.

Parameter	value
pH	6.8
Na	7,450 mg/l
Ca	14,800 mg/l
HCO_3^-	42 mg/l
Fe(2)	3.45 mg/l
Cl	36,800 mg/l
(SO_4^{2-})	(1,210 mg/l)

Results of the PhreeqC simulations are shown in Figure 4-3 for the aqueous phase activities of Fe^{2+} and carbonate species plotted as a function of H_2 partial pressure and in Figure 4-4 as a function of $Fe_{(cr)}$ reacted. Figure 4-5 shows the effect of H_2 partial pressure on the theoretical equilibrium potentials calculated using Equation 4-1 and the PhreeqC calculated aqueous phase activities and (Peng-Robinson) H_2 gas fugacity. Figure 4-6 shows a close-up of the equilibrium potentials calculated for reactions 1, 4, 5, and 6 through 8 as well as the corresponding potentials assuming H_2 as an ideal gas and no activity corrections for pressure (broken curves). The PhreeqC calculated endpoint of H_2 production is indicated by a vertical broken line in Figure 4-5 and Figure 4-6. The corrosion process effectively halts when the partial pressure of H_2 gas reaches 68.5 MPa at which point metallic $Fe_{(cr)}$ and magnetite coexist at equilibrium. No further increase in H_2 partial pressure is thermodynamically possible beyond this point.

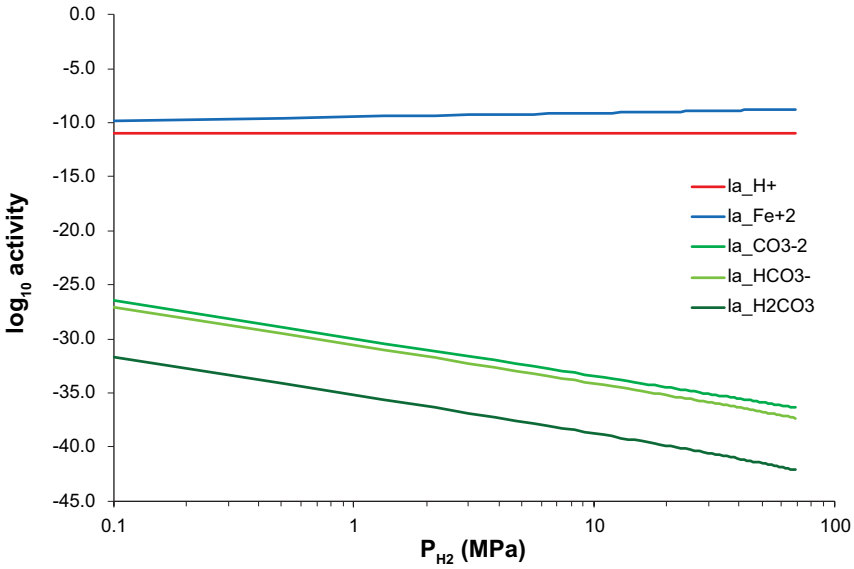

Figure 4-3. *Effect of H_2 partial pressure on groundwater species activities as calculated by PhreeqC for metallic Fe added to brine groundwater in a closed system. Temperature 25°C, pH 6.8. Calculations made using PhreeqC together with the LLNL-TDB. Precipitation of calcite, ferrous hydroxide, siderite, and magnetite permitted if oversaturated.*

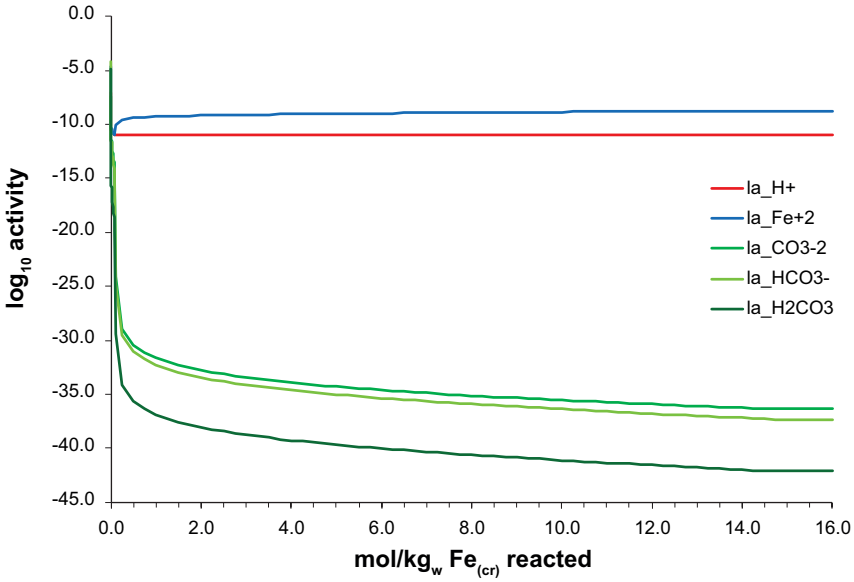

Figure 4-4. *Activities of aqueous species plotted as a function of $Fe_{(cr)}$ reacted as calculated by PhreeqC for metallic Fe added to brine groundwater in a closed system. Temperature 25°C, pH 6.8. Precipitation of calcite, ferrous hydroxide, siderite, and magnetite permitted if oversaturated.*

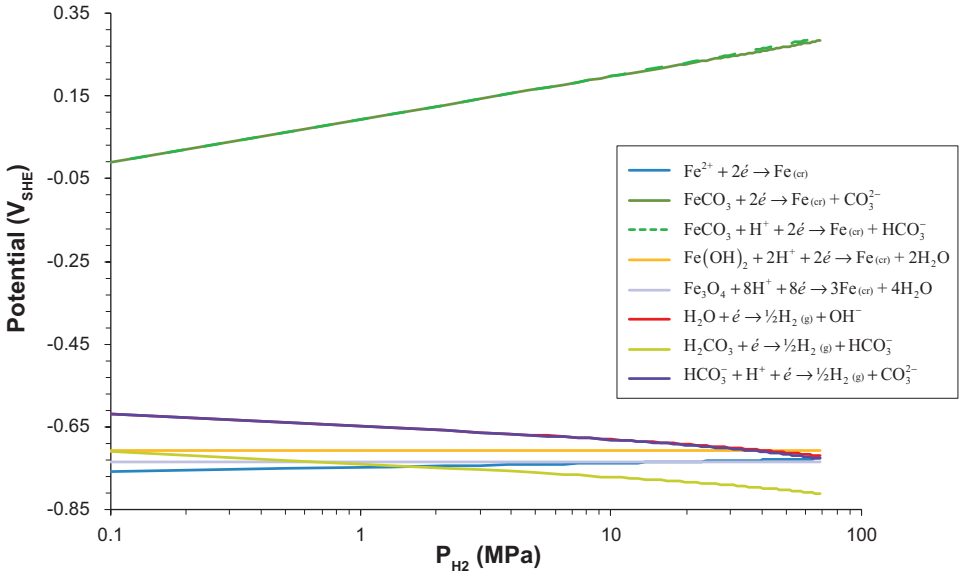

Figure 4-5. *Effect of H_2 partial pressure on the theoretical equilibrium potential (Equation 4-1) for the anodic and cathodic processes given in Table 4-1. Temperature 25°C, pH 6.8.*

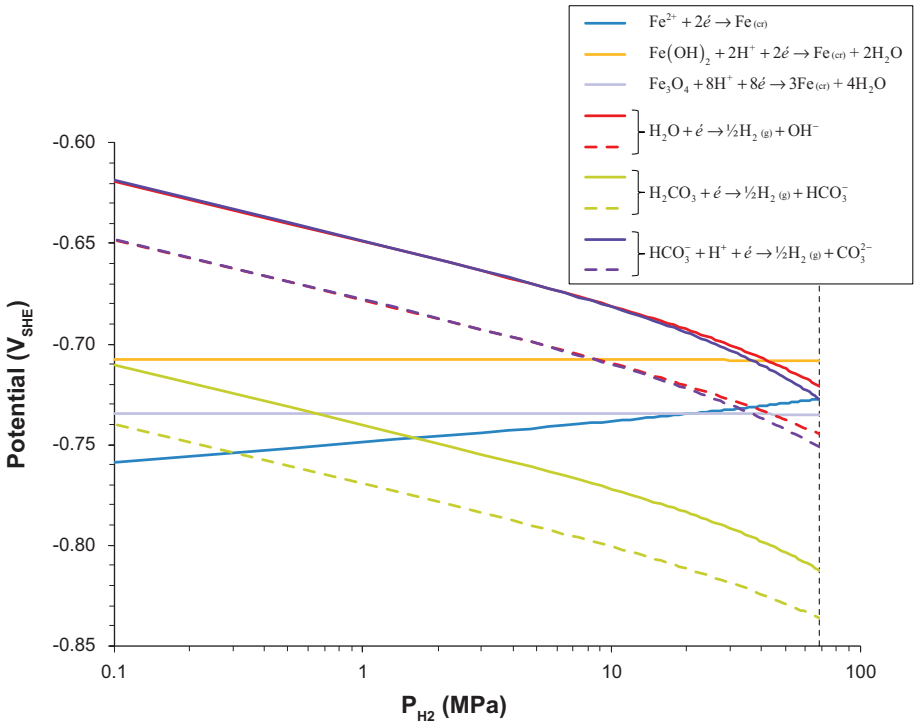

Figure 4-6. *Effect of H_2 partial pressure on the theoretical equilibrium potential for the anodic and cathodic processes in Table 4-1. Temperature 25°C, pH 6.8. Broken curves show the corresponding equilibrium potentials assuming H_2 to be an ideal gas (only cathode reactions 6–8 are affected by H_2 partial pressure). The PhreeqC calculated H_2 equilibrium partial pressure of 68.5 MPa is indicated by the vertical grey broken line.*

From Figure 4-5 and Figure 4-6 it is clear that the reduction of water is the only feasible cathodic reaction, while oxidation of $Fe_{(cr)}$ producing Fe_3O_4 (magnetite) or Fe^{2+} is the most likely anodic reaction under the simulated conditions. The theoretically calculated potentials using the Nernst equation indicate an equilibrium for the $Fe_{(cr)}|Fe_3O_4$ corrosion process at 43 MPa assuming H_2 as an ideal gas. When using the PR-EOS the equilibrium partial pressure is approximately ~115 MPa when extrapolating from the curves for reaction 1 and 6. The extrapolation is only approximate, however, since the Nernst equation calculation uses reaction component activities calculated by PhreeqC which gives a non-linear change in slope when close to the PhreeqC calculated equilibrium for the $Fe_{(cr)}|Fe_3O_4$ corrosion process.

The equilibrium H_2 partial pressure of 68.5 MPa calculated by PhreeqC is also lower than that estimated by the Nernst calculation which appears to be due to small differences between the equilibrium constants used in the LLNL database and the reaction data given in Table 4-1. There are some notable differences between the equilibrium simulated in this section and the simplified calculations described in Section 4.1. The key difference, however, is the fact that the composition of the groundwater is significantly affected by the Fe corrosion reaction in the present case giving both an elevated pH ~11, decreased activity of Fe^{2+}, and extremely low activity of carbonate species owing to the impact of calcite equilibrium at high pH (see Figure 4-3 and Figure 4-4). The high pH conditions effectively rule out formation of siderite as a corrosion product and, when coupled with the much lower Fe^{2+} activity, decrease the equilibrium H_2 partial pressure for the $Fe_{(cr)}|Fe_3O_4$ corrosion process as calculated by the Nernst equation.

If we additionally consider the effect of elevated temperature at disposal depth in a deep borehole it is necessary to make additional corrections to the equilibrium constants. For reactions that have an approximately constant enthalpy of reaction, the Van't Hoff expression (Langmuir 1997) can be used to estimate reaction constants at temperatures other than 25°C (298.15 K):

$$\log_{10} K_{(T)} = \log_{10} K_{(T_0)} - \frac{\Delta H_r^0}{(2.303) R}\left(\frac{1}{T} - \frac{1}{T_0}\right) \quad (4\text{-}4)$$

Where, T_0 (K) and T (K) are the reference and local borehole temperatures, R is the universal gas constant (8.3145×10^{-3} kJ/mol·K), and ΔH_r^0 (kJ/mol) is the enthalpy of reaction at the reference temperature. Reaction stoichiometries written in iso-coulombic form (i.e. reactions 2, 3, 6, and 7 in Table 4-1) typically have relatively constant reaction enthalpies since electrostatic interactions between ionic species and water tend to have the strongest influence on the enthalpy of a reaction (Puigdomenech et al. 1999).

As explained by Langmuir (1997) use of the Van't Hoff expression for reactions having non-constant reaction enthalpies implies an error that may be significant at elevated temperatures (i.e. ≥ 50°C). For reactions that are not defined in iso-coulombic form (i.e. reactions 1, 4, and 5 in Table 4-1) an empirically fitted analytical expression is typically used to give the variation of the equilibrium constant as a function of temperature:

$$\log_{10} K_{(T)} = A + B \cdot T + \frac{C}{T} + D \cdot \log_{10} T + \frac{E}{T^2} \quad (4\text{-}5)$$

The LLNL-TDB thermodynamic database contains reaction enthalpies as well as parameters for the analytical expression given in Equation 4-5 where available. Neither Peng-Robinson EOS parameters for gas phases nor molar volumes of species and solid phases are given in the LLNL-TDB, so extrapolations to higher pressures are not possible unless additional modifications are made by additionally specifying the critical temperature (33.2 K), critical pressure (1.3 MPa) and acentric factor (–0.225) for H_2 gas.

In the present case, temperature corrections are deemed important since the approximate 13–16°C/km (Marsic and Grundfelt 2013) temperature rise with depth implies in situ temperatures just short of 100°C at 5 km depth. Parameters for the PR-EOS have been included as additional definitions in the input file for the H_2 gas phase. Key reactions in the groundwater system were modified by including molar volumes to enable pressure corrections to equilibrium constants according to Equation 4-3. The inclusion of molar volumes for key groundwater components also allows the density of the groundwater to be calculated by PhreeqC (Appelo et al. 2014). All modifications are included in the header of the simulation input files and override the corresponding values given in the database.

Figure 4-7 shows results of calculations made using PhreeqC and assuming either an ideal gas or the Peng-Robinsom EOS for H_2. Equilibrium constants of reactions and consequently, the equilibrium H_2 partial pressure are also significantly affected by the net change in molar volume of reactants and products (Equation 4-3) and cannot be neglected. Sensitivity calculations indicate that the molar volumes of the mineral phases overwhelmingly dominate the magnitude of the pressure corrections while molar volumes of dissolved species play a relatively minor role. Using the Peng-Robinson EOS, the equilibrium partial pressure of H_2 is calculated to vary from 68.5 MPa at ambient temperature to approximately 108 MPa at 100°C.

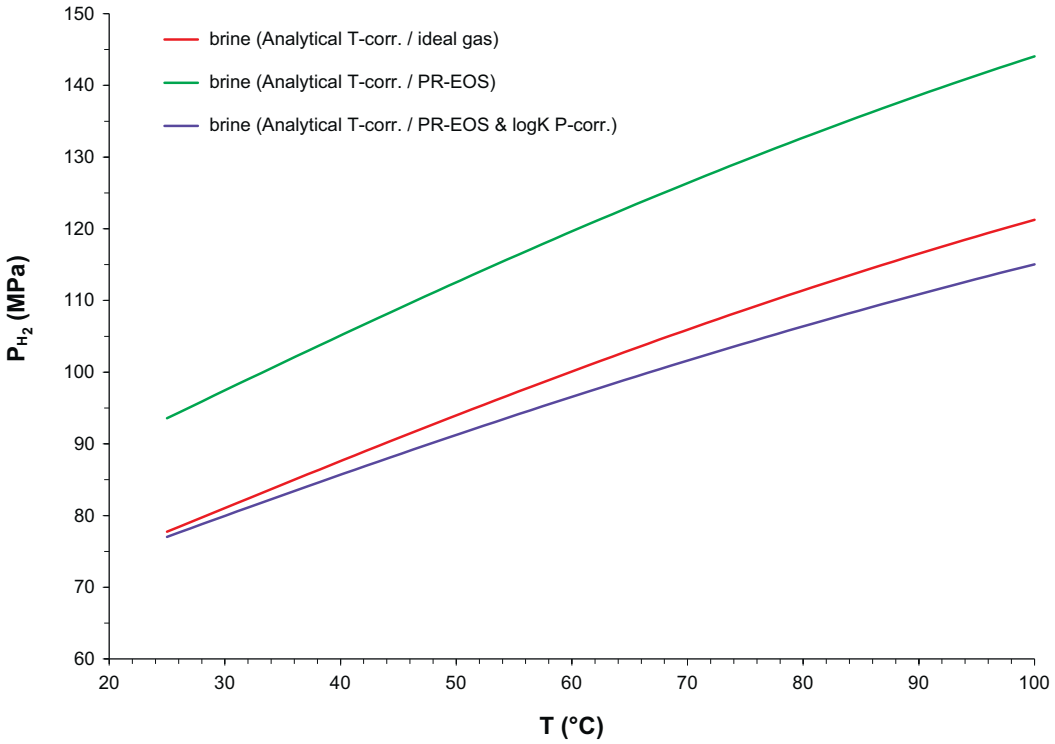

Figure 4-7. *Effect of temperature on the equilibrium H_2 partial pressure calculated by PhreeqC using the LLNL-TDB. Calculations made using the Peng-Robinson EOS (green curve) give higher equilibrium H_2 partial pressures than assumption of an ideal gas (red curve). Pressure effects on conditional equilibrium constants play a significant role to reduce the equilibrium H_2 partial pressure (purple curve).*

5 Rate of H_2 gas generation

5.1 Gas generation in a compartmentalised borehole

As the corrosion reaction proceeds, the H_2 partial pressure increases until it reaches the local hydrostatic pressure. After the point when H_2 partial pressure exceeds the hydrostatic pressure, gas bubbles will form if the water can be displaced through flow bearing fractures or through the annulus between the perforated borehole casing and the rock. Flow may also occur through the rock matrix if there is non-zero permeability and the pressure in the borehole is higher than the capillary pressure in the rock matrix.

Even if the pressure of generated gas is such that the water in the borehole is displaced entirely, the rate of gas generation should remain relatively unchanged since there will always be a film of saturated water at the corroding metal surface that is constantly replenished by diffusive transport of water vapour. Below, the equations for the rate of gas generation assuming a compartmentalised borehole are derived. In Section 5.2 the equations are adapted and solved for the case of a perforated casing in the disposal zone described in Chapter 2 and the resulting rate of gas generation is estimated.

Assuming that the far-from equilibrium rate of gas generation at high pressure can be taken to be approximately the same as that measured in laboratory investigations (typically at much lower pressures), the net rate of gas production can be estimated using a TST-type (*Transition State Theory*) kinetic expression (Lasaga 1981, 1984) and the defined stoichiometry of the corrosion reaction. Although more complex expressions can be derived, by far the simplest approach is to combine the far-from equilibrium rate of corrosion together with the specific surface area of corroding steel and a simplified driving force term to account for the slowdown in the rate of gas generation as the reaction approaches equilibrium. One such expression is:

$$R_{H_2} \approx \frac{4}{3}\left(\frac{r_{Fe}^0}{V_m}\right) A_0 \left(1-\Omega_{H_2}\right) \tag{5-1}$$

Where,

$$\Omega_{H_2} = \frac{P_{H_2}}{P_{H_2-eqm}} \tag{5-2}$$

Here, R_{H2} (mol/y) is the overall rate of gas production, r_{Fe}^0 (m/y) is the specific rate of Fe corrosion, V_m (mol/m^3) is the molar volume of corroding metal, A_0 (m^2/m) is the specific surface area of corroding steel per unit borehole length, P_{H2} (MPa) is the actual H_2 gas pressure, while $P_{H2\text{-}eqm}$ (MPa) is the equilibrium partial pressure of H_2 for the corrosion reaction. The multiplying factor 4/3 accounts for the stoichiometry of corrosion Equation 3-3 where 1.33 moles of H_2 gas are produced per mole of $Fe_{(cr)}$ reacted. Strictly speaking, this expression is only an approximation since one should actually use the fugacity of H_2 gas rather than pressure in Equation 5-2. Since the slowdown in gas generation will be most prominent at pressures close to equilibrium, however, the fugacity coefficient can be assumed to be roughly equal in both the numerator and denominator of Equation 5-2. If this is the case, the fugacity coefficient cancels out leaving the pressure ratio.

Some far-from-equilibrium rates r_{Fe}^0 of anoxic corrosion reported in the literature are given in Table 5-1.

Table 5-1. Summary of anoxic corrosion rates for candidate container/casing materials for the Deep Borehole Disposal concept.

Alloy	Anoxic corrosion rate (µm/y)*	Comment	Reference
Stainless steel, including Ni-based alloys such as Alloy 825	0.01–1	The high salinity and high temperature could result in reasonably high corrosion rates. The lower end of the range would be applicable if the pH was elevated because of the presence of concrete.	Blackwood et al. (2002), King and Watson (2010), Wada and Nishimura (1999)
Higher Ni alloys, such as Hastelloys, Alloy 625	0.01	Highly corrosion resistant due to their high Cr contents (up to 23 wt.%) and the additions of W and/or Co.	DOE (2008), Hua and Gordon (2004)
Ti alloys	0.01	Highly corrosion resistant due to the formation of a passive TiO_2 film.	DOE (2008), Hua and Gordon (2004)
Zr and similar "valve metals"	0.001–0.01	Highly corrosion resistant due to the formation of a passive ZrO_2 film.	Hansson (1985), Wada and Nishimura (1999)
C-steel	0.1–10	The lower end of the range corresponds to alkaline solutions. The upper end of the range could be slightly higher in saline water at 60–100°C.	King and Stroes-Gascoyne (2000)

* 60–100°C, saline ground water.

From Table 5-1 a far-from equilibrium corrosion rate ranging from 0.01–10 µm/y seems reasonable for most steel alloys likely to be used in construction of a deep borehole disposal system.

5.2 Estimation of gas generation in a borehole with a perforated casing

The borehole design concept under study for disposal in deep boreholes includes using a perforated casing in the disposal zone, i.e. between three and five kilometres depth. In this case, the total gas generation in the borehole can be estimated from Equation 5-1 where P is the local hydrostatic pressure in the borehole. Here, it is assumed that gas is generated at the prevailing hydrostatic pressure for that depth and efficiently displaces an equal volume of water without causing an additional pressure rise. The local volumetric rate of H_2 gas generation is

$$\frac{dv_{H_2}}{dt} = \frac{RT}{P} \cdot \frac{1}{Z_c} \cdot R_{H_2} \tag{5-3}$$

Where T and P are the local temperature and pressure at a given location in the borehole, Z_c is the compressibility of H_2 gas, and R_{H2} is the molar rate of gas production. The total volumetric rate of gas production in the borehole can be obtained by integrating the local rate over the length of the corroding steel canisters and borehole casings. Under steady state conditions, the total volume of gas exiting at the top of the borehole at ambient conditions (T_0 = 298 K, P_0 = 0.1 MPa) would then be:

$$\frac{dV_{H_2}}{dt} = \frac{RT_0}{P_0} \cdot A_0 \cdot \int_{z_0}^{L} R_{H_2}(z)\, dz \tag{5-4}$$

Where A_0 (m^2/m) is here taken to be the average specific surface area of the corroding steel casing per unit length of borehole, L (m) is the total borehole depth, and z_0 (m) is the depth at which the corrosion of steel begins. Since the gas is released at atmospheric temperature and pressure at the top of the borehole, the volume can be calculated to a good approximation using the ideal gas law (Z_c = 1). The local hydrostatic pressure in the borehole at depth h (m) is given by:

$$P = P_0 + g_c \int_0^L \rho_w(z)\, dz \tag{5-5}$$

If one were to assume an average fluid density for the borehole, this expression would simplify to:

$$P(z) \approx P_0 + \overline{\rho}_w g_c z \tag{5-6}$$

Where,

$$\overline{\rho}_w = \frac{\int_0^L \rho_w(z)\,dz}{L} \tag{5-7}$$

Since the partial pressure of H_2 gas generated is assumed to be equal to the local hydrostatic pressure, we can write:

$$\frac{dV_{H_2}}{dt} = \left(\frac{RT_0}{P_0}\right)\cdot\frac{4}{3}\left(\frac{r_{Fe}^0}{V_m}\right)A_0 \int_{z_0}^{L}\left(1-\Omega(z)\right)dz \tag{5-8}$$

This can be written in terms of an average approach to equilibrium driving force in the deposition interval:

$$\frac{dV_{H_2}}{dt} = \left(\frac{RT_0}{P_0}\right)\cdot\frac{4}{3}\left(\frac{r_{Fe}^0}{V_m}\right)A_0 \cdot \left(1-\Omega\right)_{av}\left(L-z_0\right) \tag{5-9}$$

Where,

$$\left(1-\Omega\right)_{av} = \frac{\int_{z_0}^{L}\left(1-\Omega(z)\right)dz}{L-z_0} \tag{5-10}$$

Making use of Equation 5-6 we then have:

$$\left(1-\Omega\right)_{av} \approx \frac{\int_{z_0}^{L}\left(1-\frac{P_0+\overline{\rho}_w g_c z}{\overline{P}_{H_2-eqm}}\right)dz}{L-z_0} \tag{5-11}$$

Where $\overline{P}_{H_2-eqm}$ is the average H_2 equilibrium partial pressure in the borehole. In the borehole the temperature would be expected to vary from perhaps 10–12°C in the near surface to about 92°C at 5 km depth assuming a depth trend of 16°C/km. The average equilibrium H_2 pressure in the depth range 3–5 km would then be somewhere between about 97 MPa and 112 MPa. Equation 5-11 can be integrated analytically to give:

$$\left(1-\Omega\right)_{av} \approx \left(1-\frac{P_0}{\overline{P}_{H_2-eqm}}\right)-\frac{\overline{\rho}_w g_c\left(L^2-z_0^2\right)}{2\left(L-z_0\right)\overline{P}_{H_2-eqm}} \approx 1-\frac{\overline{\rho}_w g_c\left(L^2-z_0^2\right)}{2\left(L-z_0\right)\overline{P}_{H_2-eqm}} \tag{5-12}$$

If one were to neglect altogether the reaction rate limitation imposed by the approach to equilibrium partial pressure of H_2 gas (i.e. $\Omega_{av} = 1$), the rate of gas production would be given simply by the expression:

$$\frac{dV_{H_2}}{dt} \approx \left(0.0245\right)\cdot\frac{4}{3}\left(\frac{r_{Fe}^0}{V_m}\right)A_0 \left(L-z_0\right) \tag{5-13}$$

Although the rate of gas generation given by Equation 5-8 can be calculated numerically in a straight-forward manner, a quick estimate can be obtained using either Equation 5-9 or 5-13 (if equilibrium approach is neglected).

5.2.1 Specific surface area of corrosion susceptible steel

The specific surface area of corrosion susceptible steel is equal to the sum of contributions from the outer surface of the emplaced steel canisters, the canister couplings, as well as the inner and outer surfaces of the well casings in the disposal zone. Here it is assumed that only the mild steel components in the disposal zone contribute to the gas generation and corrosion of components in the upper part of the borehole is neglected. Since the canister strings are interspersed periodically with 10 m concrete plugs as well as canister spacers with a slightly larger diameter to the canisters themselves, it is necessary to estimate the average specific surface area per length of borehole. If one neglects the

slight difference in diameter of the spacers and the additional surface area flange between spacers and canisters, the average specific surface area contributed by the emplaced canisters and spacers in the lower 2,000 m of the borehole is given approximately as:

$$\overline{A}_{can}\left(\mathrm{m}^2/\mathrm{m}\right) \approx 0.34\,\pi\left(\frac{2000-100}{2000}\right) = 1.015 \tag{5-14}$$

Assuming that the borehole casing in the concrete plugged sections does not corrode as fast as that in the emplacement sections and can therefore be neglected, the average specific surface area contributed by the borehole casing is:

$$\overline{A}_{case}\left(\mathrm{m}^2/\mathrm{m}\right) \approx \left(0.406+0.381\right)\pi\left(\frac{2000-100}{2000}\right) = 2.349 \tag{5-15}$$

The average, total specific surface area of readily corrosion susceptible steel in the deposition zone is therefore:

$$A_0\left(\mathrm{m}^2/\mathrm{m}\right) \approx 1.015 + 2.349 = 3.364 \tag{5-16}$$

5.2.2 Density of borehole groundwater

In the present analysis, a simplified approach is taken whereby the salinity of groundwater is assumed to increase from effectively fresh water in the near surface to brine at 1,000 m depth. If the salinity profile is assumed to vary linearly and brine of constant composition (Table 4-2) resides at depths greater than 1,000 m, it is relatively straight-forward to calculate the density of groundwater in the borehole. On top of this, consideration must also be given to the temperature and, to a lesser extent, pressure increase with increasing depth as this also has a non-negligible impact on density. The variation of density as a function of depth where consideration is given to both temperature and pressure is shown in Figure 5-1. Calculations for brine are made using PhreeqC while the density variation of pure water is estimated using the correlation given by Sharqawy et al. (2010).

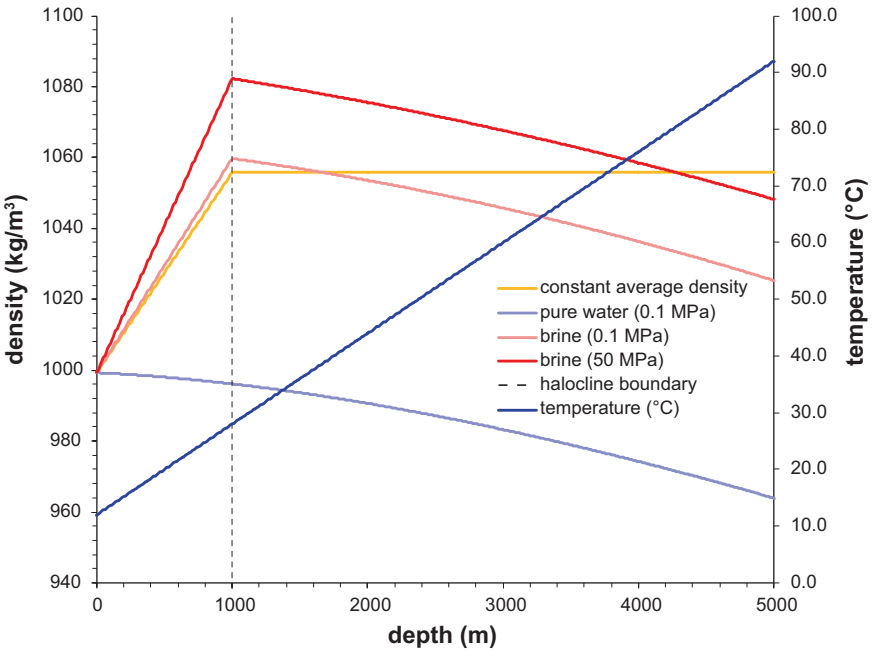

Figure 5-1. *Impact of temperature and pressure on density of groundwater as a function of depth assuming a halocline at 1,000 m depth and constant temperature increase of 16°C/km from a near surface temperature of 12°C. For comparison, curves are shown for pure water (0.1 MPa), brine (0.1 MPa and 50 MPa), as well as for an assumed constant density (equal to the average of the two brine curves at depth greater than 1,000 m).*

5.2.3 Net gas generation rate

Parameters necessary to evaluate the gas production rate using Equations 5-9 to 5-13 are given in Table 5-2.

The value of the equilibrium approach factor, $(1\text{-}\Omega)_{av}$ calculated using the approximation given in Equation 5-12 is thus:

$$\left(1-\Omega\right)_{av} \approx 1-\frac{1056\left(9.807\right)\left(5000^2-3000^2\right)}{2(5000-3000)104.5\times10^6}=0.604 \qquad (5\text{-}17)$$

This is almost the same as the value (Ω_{av} = 0.601) calculated by proper numerical integration of Equation 5-10 (see Figure 5-2) in the interval 3–5 km suggesting that the use of an arithmetic average for the equilibrium H_2 partial pressure and groundwater density gives acceptable accuracy. The rate of gas production therefore should be about 60% of the maximum rate in the absence of the equilibrium driving force limitation. As can be seen from Figure 5-2 very little increase in accuracy is attained by using more exact estimates of the groundwater density over that obtained by assuming pure water (~10% error), although the assumption of an ideal gas would have a more significant impact on the estimated equilibrium approach.

If no limitation on gas generation due to equilibrium approach is imposed, then the maximum total rate of gas generation (i.e. exiting at the top of the borehole) would be:

$$\frac{dV_{H_2}}{dt}=0.0245\left(\frac{4\left(3.364\right)\left(5000-3000\right)}{3\left(7.09\times10^{-6}\right)}\right)\cdot r_{Fe}^0=\left(3.095\times10^7\right)r_{Fe}^0 \qquad (5\text{-}18)$$

Where the corrosion rate, r_{Fe}^0 is specified in units of m/y. For a corrosion rate in the range 0.01–10 µm/y, the maximum total rate of gas generation would therefore be in the range 0.3–310 m^3/y. Considering the reduction in the rate of corrosion due to equilibrium approach would give a range of 0.19–186 m^3/y for the same corrosion rates.

The local specific volumetric rate of H_2 gas generation (m^3/m y) is plotted in Figure 5-3 together with the corresponding time required to completely displace the water filled annulus after steady state conditions have become established. As can be seen from the Figure, the in-situ hydrostatic pressure has a significant impact on the volumetric rate of gas generation even though the molar rate of gas generation does not vary by more than a factor of two over the length of the deposition zone. The void volume in the borehole mud is 20–25 litres per metre of borehole corresponding to a 40–50% void fraction. This means that the gas generated at 5 km depth (2.5×10^{-4} m^3/m y) will be able to displace this void volume in about 80–100 years after steady state conditions have been attained.

Figure 5-4 shows the total time required to completely fill the water-filled borehole annulus with H_2 gas for an assumed void fraction of 50% including the initial transient period until the borehole water reaches saturation with respect to dissolved H_2. At a depth of 3,000 m, the hydrostatic pressure and temperature are 30.9 MPa and 60°C. Under these conditions, the maximum dissolved concentration of H_2 is 0.21 mol/kgw. For a corrosion rate of 10 µm/y, it would take 1.3 y to reach H_2 saturation in the aqueous phase, after which the concentration remains constant and free phase gas bubbles can form. After this steady-state condition is reached it would take a further 54 years for the free phase H_2 gas to completely displace the water from the borehole annulus.

At a depth of 5,000 m, the hydrostatic pressure and temperature are 52 MPa and 92°C. Under these conditions, the maximum dissolved concentration of H_2 is 0.39 mol/kgw which is roughly double that calculated for 3,000 m depth. At this depth it will take roughly 2.9 y to reach the steady state concentration and then a further 103 y to completely displace the water from the borehole annulus.

As the gas continues to form, it is likely to find preferential paths through the borehole mud. As a consequence the plug flow displacement scenario outlined above is less plausible.

Table 5-2. Summary of input data necessary to estimate the gas generation rate due to steel corrosion in the Deep Borehole Disposal concept using Equations 5-9 to 5-13.

Parameter	value	Comments
A_0	3.364 m^2/m	Area per unit length of borehole in disposal interval
L	5,000 m	End of deposition zone
z_0	3,000 m	Start of deposition zone
V_m	7.09×10^{-6} m^3/mol	Molar volume of steel
r_{Fe}^0	0.01–10 µm/y	Rate of corrosion
$\overline{\rho}_w$ (z > 1,000 m)	1,056 kg/m^3	Arithmetic average density below halocline
g_c	9.807 m/s^2	Acceleration due to gravity
$\overline{P}_{H_2-eqm}$	104.5 MPa	Arithmetic average in depth interval 3–5 km
Ω_{av}	0.601	Calculated by quadrature in depth interval 3–5 km

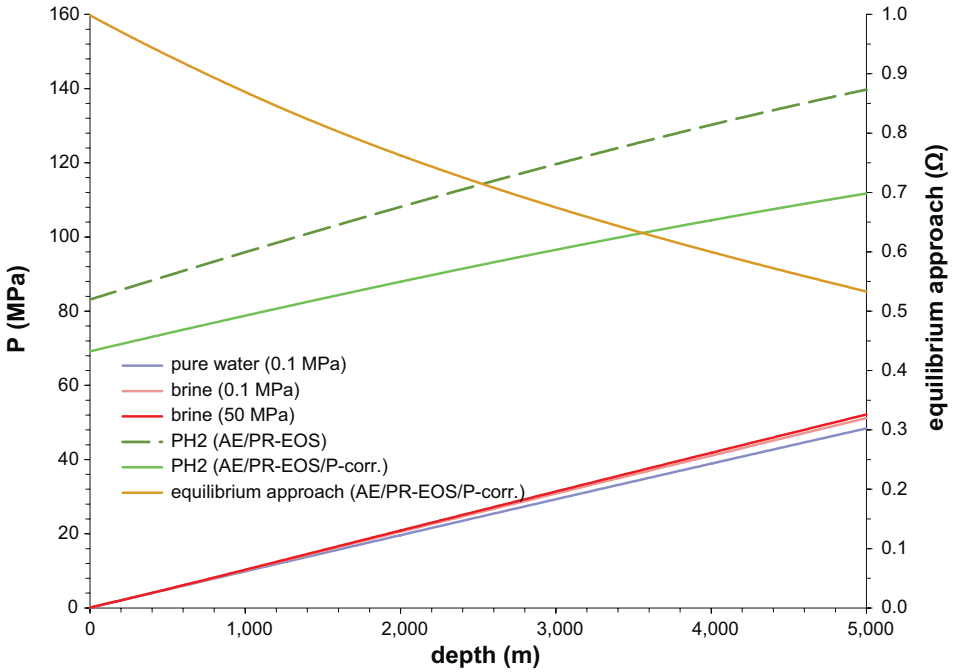

Figure 5-2. *Plot of equilibrium H_2 partial pressure (PR-EOS with and without additional pressure correction of equilibrium constants), hydrostatic pressure (pure water and brine at two different hydrostatic pressures), as well as reduction factor for the rate of as generation due to equilibrium approach.*

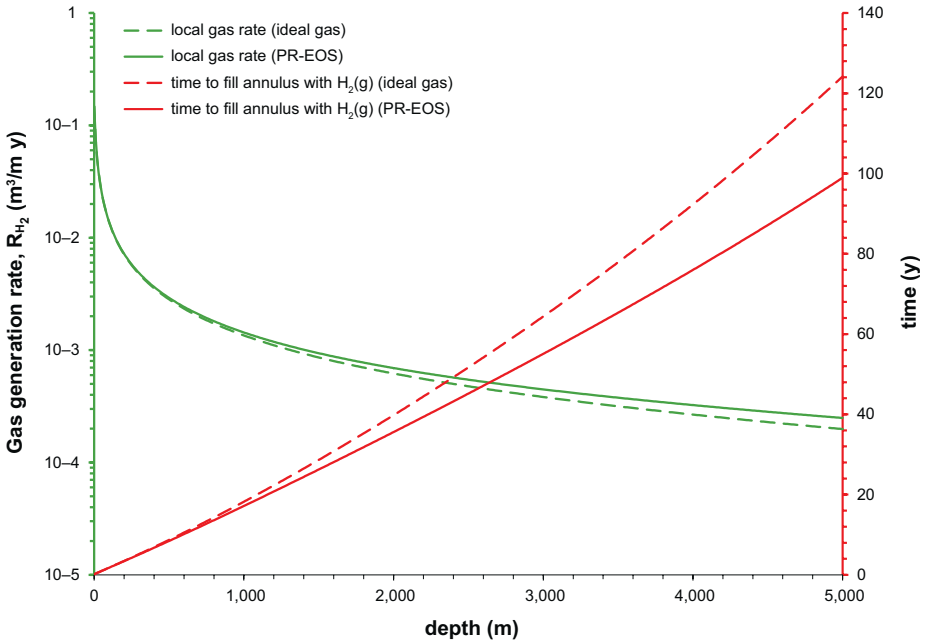

Figure 5-3. *Local specific volumetric rate (Equation 5-3) of gas generation (m^3/m y) and time (y) to displace water in borehole annulus (50% void volume) at different depths assuming an ideal gas (broken curves) and for a compressible gas using the PR-EOS for H_2 (unbroken curves). Time for reaching steady state dissolved hydrogen concentration not included. Assumed corrosion rate 10 µm/y.*

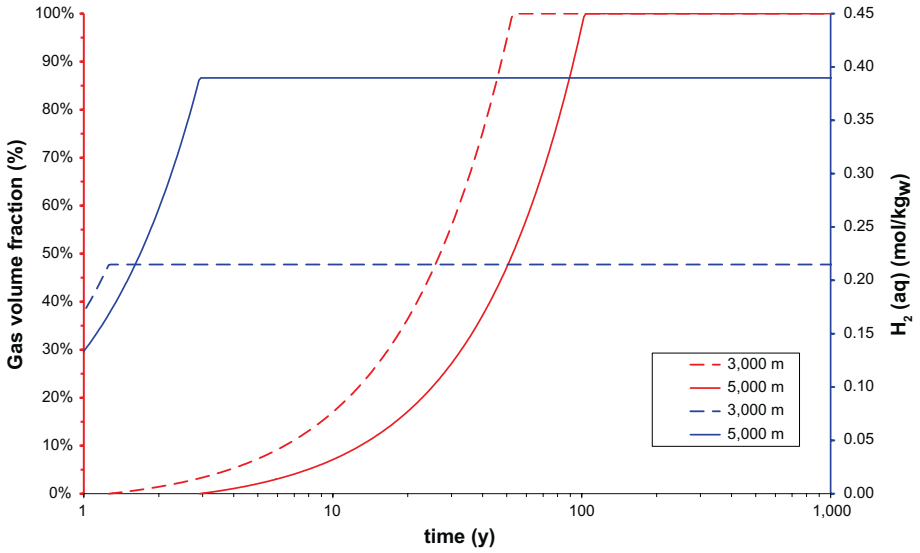

Figure 5-4. *Total time (y) to displace water in borehole annulus (50% void volume) for a corrosion rate of 10 µm/y at different depths (assuming the PR-EOS for H_2). The left-hand axis (red curves) shows the local gas volume fraction as a function of time while the right-hand axis (blue curves) shows the corresponding aqueous phase H_2 concentration.*

5.3 Other materials

Corrosion rates for a variety of different materials are given in Table 5-1. Most likely canisters can be fabricated using, for example, nickel alloys, titanium alloys or other metals with a better corrosion resistance than that of mild steel (C-steel). However, using these metals also for the borehole casing will probably be extremely expensive. Also, it needs to be clarified if such materials would have the mechanical and other properties (e.g. hydrogen embrittlement resistance) necessary to render them suitable as casing materials.

6 Discussion

In this report, a model for the formation of hydrogen from corrosion of steel canisters and borehole casing tubes used for depositing spent nuclear fuel in deep boreholes is presented. The results show that the most likely corrosion mechanism is a reaction between the iron in the steel and the water in the borehole leading to the formation of magnetite and hydrogen. It is demonstrated that the equilibrium hydrogen pressure, i.e. the pressure at which the oxidation of iron halts, significantly exceeds the hydrostatic pressure in the borehole. Hence, the corrosion of the steel is expected to continue until all iron has been consumed.

Based on literature data the anaerobic corrosion rate for steel is judged to fall in the interval 0.01–10 µm/year where the lower end of the interval represents stainless steel at a high pH, e.g. a cementitious environment, while the upper end is judged to be applicable to mild steel in a warm and saline environment. Under the conditions expected in the disposal zone of a deep borehole, i.e. mild steel in a calcium dominated brine (5–10 % salt content), temperatures in the interval 60–100°C and a hydrostatic pressure in the range 30–50 MPa, the rate of hydrogen formation is estimated to be about 186 m^3 (STP) per year accounting for a rate reduction due to the pressure of the hydrogen formed.

At first, the hydrogen formed will dissolve in the water in the borehole. Due to the pressure and temperature difference between the upper part of the disposal zone (3 km depth, ~30 MPa and ~60°C) and the bottom (5 km depth, ~50 MPa and ~90°C) the solubility of hydrogen in the water varies between about 0.2 and 0.4 moles per kg of water. The hydrogen formation will lead to that these solubility limits are estimated to be exceeded after between 1.3 (3 km depth) and 2.9 years (5 km depth). After this point in time, bubbles of free phase hydrogen will be formed on the steel surfaces.

At the high hydrostatic pressures encountered at 3–5 km depth, free phase H_2 will exist as a super-critical fluid with transport properties bearing similarity to both a liquid and a gas. In spite of the high solubility of H_2 gas under these conditions there appears to be no risk of formation of a single miscible phase (see e.g. Rimbach and Chatterjee 1987) and the pressures are far below that required for clathrate formation (Lee et al. 2005).

We have not checked the robustness of the PhreeqC H_2-H_2O gas-liquid equilibrium calculation against independent VLE data. However, it has been shown to be accurate for the more non-ideal CO_2-H_2O system (Appelo et al. 2014). Hence, it is reasonable to expect that it should hold also for H_2-H_2O. The average implied Henry's constant of ~10^5 (atm./mol-fraction H_2) used by PhreeqC in the temperature and pressure interval being considered is also roughly the same order of magnitude as that reported by Prausnitz (1968) further supporting this claim.

Given the complexity of the three-phase system comprised of borehole mud, water, and gas the hydrogen flow process may not be possible to predict à priori. Consequently, the dimensions and number of rising bubbles will be very uncertain. Precedents exist in the Chemical Engineering literature where such multiphase flow systems have been modelled semi-empirically. This work is mostly in relation to gas-liquid mass transfer or prediction of flooding in packed gas-liquid contacting columns or air-lift reactors (see, e.g. Perry and Green 1987). In most cases where one considers a dispersed gas in a continuous liquid phase, a population of bubbles of constant size is assumed. Since the dispersed phase is usually generated in industrial applications using a sparger or similar mechanical device with well-known characteristics, it is usually not necessary to model the dynamics of bubble formation and detachment in detail as would the case here.

In general, multiphase "bubbly" flow is very difficult to simulate, particularly when there is a large difference between the densities of the continuous and dispersed phases, although there are specialised numerical CFD (*Computational Fluid Dynamics*) tools that can be used for this. Generally, these are based upon idealised representations based on volume averaging techniques where the bubbles are assumed to be simple, non-deformable and non-coalescing spheres and the hydrodynamic problem is approximated as single phase flow system. The hydrodynamic drag forces on individual bubbles are typically modelled using an approximate k-ε (eddy viscosity) type model, given that the Reynolds number is sufficiently high that turbulent conditions exist.

The present situation where rising bubbles experience a significant pressure drop over the depth of the borehole leading to volumetric expansion may be very difficult to handle even if the bubbly flow can be modelled, in principle. The non-Newtonian viscous properties of the borehole mud will also add additional complexity to the physical description which will most likely be very difficult to account for.

References

SKB's (Svensk Kärnbränslehantering AB) publications can be found at www.skb.se/publications.

Appelo C A J, Parkhurst D L , Post V E A, 2014. Equations for calculating hydrogeochemical reactions of minerals and gases such as CO_2 at high pressures and temperatures. Geochimica et Cosmochimica Acta 125, 49–67.

Arnold B W, Brady P V, Bauer S J, Herrick C, Pye S, Finger J, 2011. Reference design and operations for deep borehole disposal of high level radioactive waste. SAND2011-6749, Sandia National Laboratories, Albuquerque, New Mexico.

Beswick J, 2008. Status of technology for deep borehole disposal. Report for NDA, Contract NP 01185, EPS International.

Blackwood D J, Gould L J, Naish C C, Porter F M, Rance A P, Sharland S M, Smart N R, Thomas M I, Yates T, 2002. The localised corrosion of carbon steel and stainless steel in simulated repository environments. AEAT/ERRA 0318, Dec 2002.

Crawford J, 2008. Bedrock transport properties Forsmark. Site descriptive modelling, SDM-Site Forsmark. SKB R-08-48, Svensk Kärnbränslehantering AB.

DOE, 2008. Yucca Mountain Reposiotry license application. U.S. Department of Energy, DOE/RW-0573.

Hansson C M, 1985. The Corrosion Of Steel And Zirconium In Anaerobic Concrete, Proc. Mat. Res. Soc. Symp. Vol. 50.

Hua F, Gordon G, 2004. Corrosion behaviour of Alloy 22 and Ti Grade 7 in a nuclear waste repository environment. Corrosion 60, 764–777.

King F, Stroes-Gascoyne S, 2000. An assessment of the long-term corrosion behaviour of C-steel and the impact on the redox conditions inside a nuclear fuel waste disposal container. Ontario Power Generation Nuclear Waste Management Division Report No: 06819-REP-01200-10028.

King F, Watson S, 2010. Review of the corrosion performance of selected metals as canister materials for UK spent fuel and/or HLW. Quintessa Report for the UK Nuclear Decommissioning Authority, QRS-1384J-1 Version 2.1, available from http://www.nda.gov.uk/documents/biblio/search.cfm.

Langmuir D, 1997. Aqueous environmental geochemistry. Upper Saddle River, N.J.: Prentice Hall.

Lasaga A C, 1981. Rate laws in chemical reactions. In Lasaga A C, Kirkpatrick R J (eds). Kinetics of geochemical processes. Washington, DC: Mineralogical Society of America. (Reviews in Mineralogy 8), 135–169.

Lasaga A C, 1984. Chemical kinetics of water–rock interactions. Journal of Geophysical Research 89, 4009–4025.

Lee H, Lee J-W, Kim D Y, Park J, Seo Y-T, Zeng H, Moudrakovski I L, Ratcliffe C I, Ripmeester J A, 2005. Tuning clathrate hydrates for hydrogen storage. Nature 434, 743–746.

Lemire R J, Berner U, Musikas C, Palmer D, Taylor P, Tochiyama O, 2013. Chemical thermodynamics. Vol 13a, Chemical thermodynamics of iron: part 1. Paris: OECD Publications.

Marsic N, Grundfelt B, 2013. Review of geoscientific data of relevance to disposal of spent nuclear fuel in deep boreholes in crystalline rock. SKB P-13-12, Svensk Kärnbränslehantering AB.

Odén A, 2013. Förutsättningar för borrning av och deponering i djupa borrhål. SKB P-13-08, Svensk Kärnbränslehantering AB. (In Swedish.)

Ortiz L, Volckaert G, Mallants D, 2002. Gas generation and migration in Boom Clay, a potential host rock formation for nuclear waste storage. Engineering Geology 64, 287–296.

Parkhurst D L, Appelo C A J, 2013. Description of input and examples for PHREEQC version 3 – A computer program for speciation, batch-reaction, one-dimensional transport, and inverse geochemical calculations. Techniques and Methods 6–A43, U.S. Geological Survey, Denver, Colorado.

Perry R H, Green D W, 1997. Perry's chemical engineers' handbook. 7th ed. New York: McGraw Hill.

Prausnitz J, 1968. Thermodynamics of fluid-phase equilibria at high pressures. In Drew T B, Cokelet G R, Hoopes J W, Vermeulen T (eds). Advances in chemical engineering. Vol 7. Academic Press, 139–206.

Puigdomenech I, Rard J A, Plyasunov A V, Grenthe I, 1999. TDB-4. Temperature corrections to thermodynamic data and enthalpy calculations. Le Seine-St. Germain: OECD Nuclear Energy Agency.

Reardon E J, 1995. Anareobic corrosion of granular iron: measurement and interpretation of hydrogen evolution rates. Environmental Science & Technology 29, 2936–2945.

Rimbach H, Chatterjee N D, 1987. Equations of state for H_2, H_2O and H_2–H_2O fluid mixtures at temperatures above 0.01°C and at high pressures. Physics and Chemistry of Minerals 14, 560–569.

Sharqawy M H, Lienhard J H, Zubair S M, 2010. Thermophysical properties of seawater: a review of existing correlations and data. Desalination and Water Treatment 16, 354–380.

SKB, 1992. Project on Alternative Systems Study (PASS). Final report. SKB TR 93-04, Svensk Kärnbränslehantering AB.

Smith J M, Van Ness H C, 1987. Introduction to chemical engineering thermodynamics. 4th ed. New York: McGraw Hill.

Wada R Nishimura T, 1999. Experimental study of hydrogen gas generation rate from corrosion of Zircaloy and stainless steel under anaerobic alkaline condition. Radioactive Waste Management and Environmental Remediation ASME 1999.